2022

Electric field control of confined magnetic skyrmions for energy efficient scalable nanomagnetic memory

Md Mahadi Rajib

Electric field control of confined magnetic skyrmions for energy efficient scalable nanomagnetic memory

A thesis submitted in partial fulfilment of the requirements for the degree of Master of Science in Mechanical and Nuclear Engineering at the Virginia Commonwealth University.

by

MD MAHADI RAJIB

Bachelor of Science in Mechanical Engineering, Bangladesh University of Engineering and Technology, 2016

Advisor: Jayasimha Atulasimha, Ph.D.

Professor, Department of Mechanical and Nuclear Engineering

Virginia Commonwealth University

Richmond, Virginia

December, 2022

Acknowledgement

First and foremost, I would like to extend my profound appreciation to my advisor Professor Jayasimha Atulasimha for his ongoing support of my studies and research as well as for his inspiration, advice, and vast knowledge. Without his guidance, I would not have been able to get this far or do what I accomplished while attending Virginia Commonwealth University. Being able to say that about him is an honor.

My profound appreciation goes out to Professors Supriyo Bandyopadhyay and Radhika Barua, members of my thesis committee, for taking the time to read the dissertation despite their incredibly busy schedules.

I would like to express my sincere gratitude to my fellow lab mates Dr. Dhritiman Bhattacharya, Ali Azam, Austin R. Roe, Walid Al Misba, Md Fahim F Chowdhury, and Muhammad Sabbir Alam for their helpful advice and enlightening discussions.

Last but not least, a sincere thank you to my family. Without my parents' constant support and everything they did to get me here, I would not be where I am today.

My research was supported by National Science Foundation SHF Small Grant # 1909030.

Table of Contents

List of Figures

Abstract

Electric field control of confined magnetic skyrmions for energy efficient scalable nanomagnetic memory

By Md Mahadi Rajib.

A thesis submitted in partial fulfillment of the requirements for the degree of Master of Science in

Mechanical and Nuclear Engineering at Virginia Commonwealth University.

Virginia Commonwealth University, 2022.

Major Director: Jayasimha Atulasimha, Ph.D.

Professor,

Department of Mechanical and Nuclear Engineering

Nanomagnetic random-access-memory (RAM) devices are considered one of the leading alternatives to the existing Complementary Metal Oxide Semiconductor (CMOS) based RAM devices due to inherent non-volatility and long endurance compared to other non-CMOS devices. However, new paradigms such as voltage control and spin orbit torque are being explored to write information with low errors in an energy efficient manner. Magnetic skyrmions have emerged as potentially viable paradigm for nanomagnetic memory devices because of their robustness, scalability and extremely low energy requirement for creation and manipulation. Besides, electric field induced manipulation of nanomagnets as well as magnetic skyrmions has been shown to be a promising strategy towards the implementation of ultra-low power memory devices.

One such electric field-based manipulation of magnetic states involves skyrmion mediated switching of perpendicular magnetic tunnel junctions (p-MTJs) based nanomagnetic memory devices. This is achieved by applying a voltage pulse starting from a ferromagnetic up/down state to reduce PMA, thus creating an intermediate skyrmion and subsequently annihilating the skyrmion by withdrawing the voltage pulse to achieve ferromagnetic down/up (i.e. reversed) state. However, scalability of skyrmions confined in a nanodot and skyrmion-mediated voltage-controlled switching strategy have not been completely investigated, particularly their scaling to 20 nm lateral dimension and beyond. In this study, we investigated the feasibility of scaling of perpendicular MTJs to lateral dimensions ~20nm and beyond, as well as dynamic skyrmion-mediated switching in such MTJs in the presence of room temperature thermal noise and defects/edge roughness.

Chapter 1: Introduction

Nanomagnetic memory devices are one of the most prominent technologies considered to replace CMOS-based RAM devices and lately their use in in-memory neuromorphic computing systems is being increasingly studied. This chapter begins with introducing nanomagnetic memory devices (1.1). And the following section (1.2) gives an overview of recent developments and our work on one of the nanomagnetic memory device concepts: scalability of skyrmion-mediated voltage-controlled reversal of ferromagnets.

1. 1 Nanomagnetic memory overview

The invention of silicon-based transistors in 1947 triggered a rapid development of computing systems. Afterwards, the effort on continuous miniaturization of transistors has revolutionized the semiconductor industry. Gordon Moore, the co-founder of Intel corporation, predicted in 1960's that the transistor number in a chip would continue to double in almost every eighteen months [1]. However, this trend is now unlikely to continue due to the unmanageable heat generated by miniaturized CMOS based memory device. Many low-power computing strategies have been developed by researchers to address this problem.

One of the most attractive alternatives to the CMOS-based memory devices is nanomagnetic memory devices. These devices are typically based on magnetic tunnel junctions (MTJs). An MTJ consists of three layers as shown in Fig.1 (a): a fixed layer, a free layer and a tunnel barrier (MgO layer). In MTJ, binary bits are encoded by exploiting one of the magnetic properties called tunneling magnetoresistance (TMR) [2-10]. Since TMR is dependent on the relative angle between the spin orientation of the free and the fixed layer so a memory bit can be written by switching the magnetization direction of the free layer between two stable orientations as shown in Fig. 1(b). When a small current is passed through the MTJ, the voltage measured across the MTJ is changed depending on the parallel or antiparallel orientation of the spins in the free layer relative to the fixed layer. Therefore, a readout operation can be performed on an MTJ-based memory device by passing a small current.

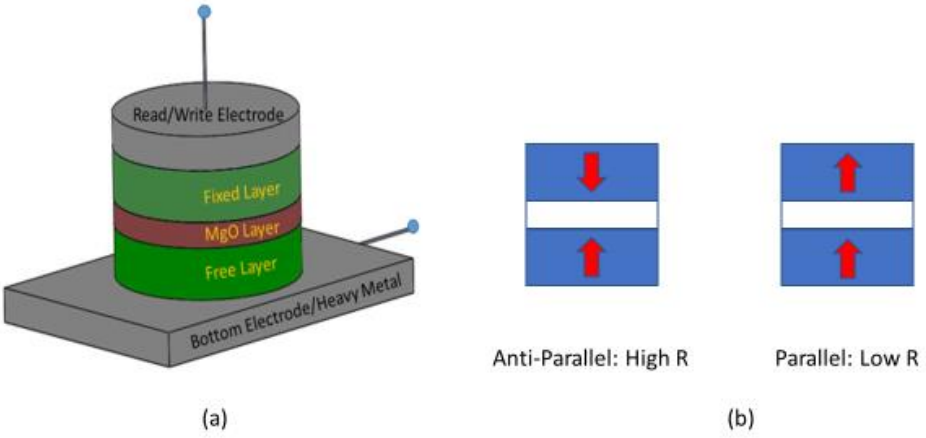

Fig. 1. (a) Schematic of an MTJ. (b) Parallel (P) and antiparallel (AP) states of MTJ corresponding to low and high magnetoresistance (binary bits).

Bistability in MTJ-based memory device can be achieved by using shape anisotropic elliptical nanomagnets or perpendicularly polarized nanomagnets in the free layer as shown in Fig. 2. The elliptical nanomagnet is typically used in the in-plane MTJs where the minimum energy state is reached when the magnetization direction is in either of the easy axis directions of the ellipse. On the other hand, perpendicularly polarized nanomagnets form the perpendicular MTJ (p-MTJ) where the easy magnetization direction is along ±z direction. However, p-MTJs are now preferred due to their scalability.

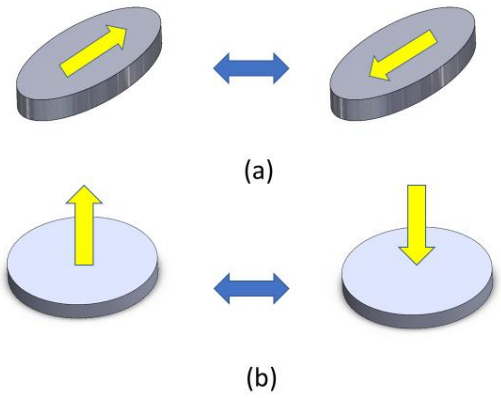

Fig. 2. (a) Elliptical nanomagnets with spins oriented along the easy axis, (b) Perpendicularly polarized circular nanomagnets used in MTJs

Various current-induced [11-15] and electric field controlled [16-23] mechanisms can be used for switching the free layer of an MTJ. Spin transfer torque (STT) [11,12] is one of the most

commonly employed current-controlled switching strategies. In STT, while passing spin current through a nanomagnet, spin polarized electrons transfer their spin angular momentum to the spins of the nanomagnet [11-13]. A spin transfer torque is induced by the spin angular momentum on nanomagnet's magnetization and it can be used to switch a nanomagnet's magnetization to a desired direction. Unpolarized incoming electrons are polarized parallel to the reference layer's magnetization while passing through the reference layer/hard layer as shown in Fig. 3(a). Thus, hard layer injects spin polarized current to the soft layer which in turn transfers the angular momentum to the electrons in the soft layer and ultimately aligns those spins in the parallel direction of hard layer's magnetization. By reversing the current direction, the magnetization directions can be aligned antiparallel to each other as shown in Fig. 3(b). In this case, the unpolarized incoming electrons are passed through the soft layer. When the electrons are injected to the hard layer, spins those are parallel to the hard layer's magnetization are transmitted. On the other hand, spins antiparallel to hard layer magnetization are reflected back to the soft layer and become majority spins over time. Thus, magnetization in the soft layer antiparallel to hard layer's magnetization direction is stabilized. So, by choosing the appropriate current direction a memory bit can be written in MTJs. However, STT switching causes a large energy dissipation (~100 fJ/bit) even when the MTJ is experimentally scaled to ~11 nm lateral dimensions [24]. For comparison, energy dissipated in CMOS devices is approximately 100 aJ/bit [25], which is nearly three orders of magnitude lesser than energy dissipated in STT-based switching.

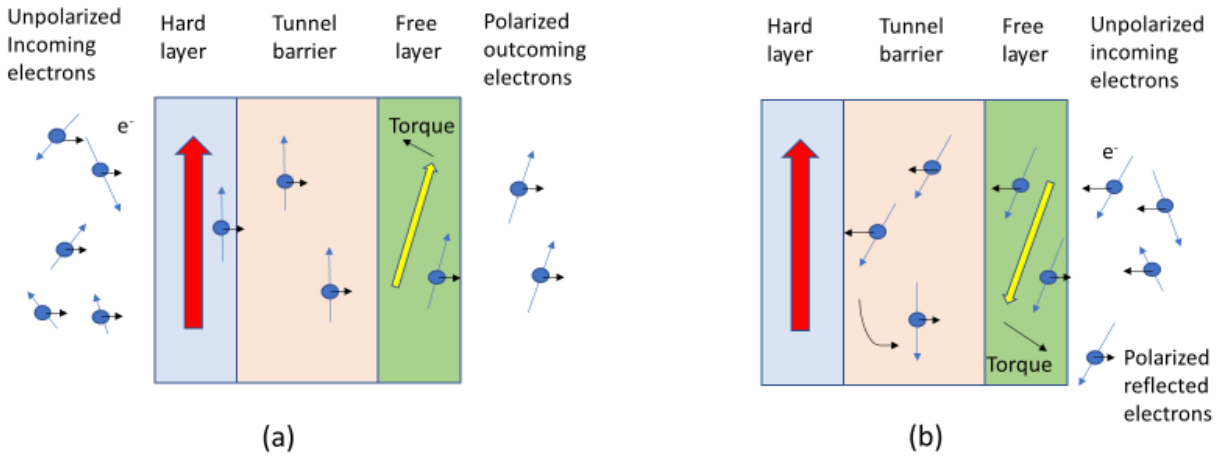

Fig. 3. Schematic illustration of STT switching mechanism. (a) AP to P switching, (b) P to AP switching

On the other hand, electric field-induced magnetization reversal is highly energy efficient. In particular, voltage-controlled magnetic anisotropy (VCMA)-based switching dissipates only ~1 fJ/bit [20, 26]. In this method, a voltage pulse alters the perpendicular magnetic anisotropy (PMA) that originates at the interface of ferromagnet/oxide [27]. By utilizing an appropriate combination of in-plane bias magnetic field and voltage pulse duration, a complete ferromagnetic reversal can be achieved [17]. However, VCMA-induced switching is precessional in nature and highly susceptible to disorders in the presence of room-temperature thermal noise [28], which is shown in Fig. 4. In contrast, it has been shown that skyrmion mediated reversal is robust to thermal noise and disorder. In this thesis, we studied the scalability of skyrmion mediated switching in scaled MTJs to 20nm and beyond in the presence of room temperature thermal noise and defects.

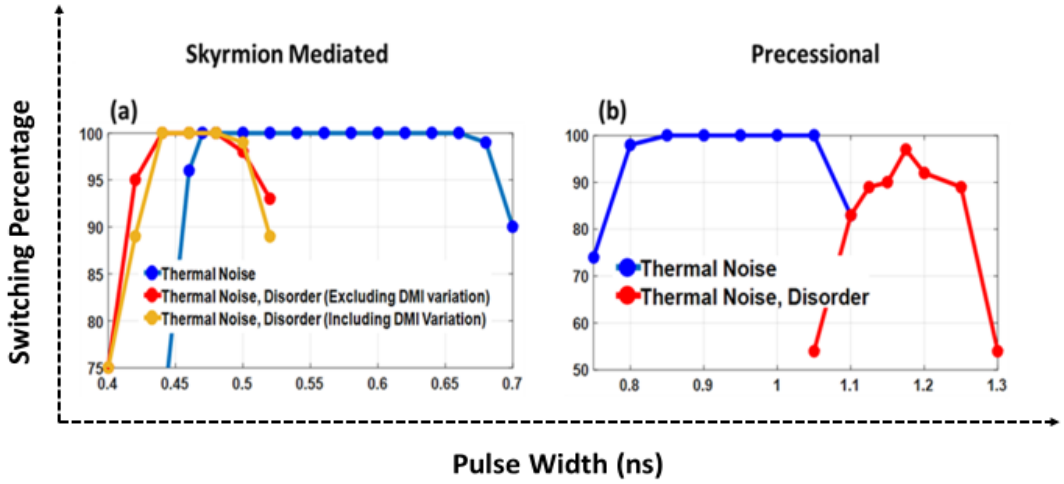

Fig. 4. Switching probability in (a) skyrmion-mediated and (b) precessional VCMA switching scheme in the presence of room-temperature thermal noise and disorder. (Figure is taken from ref [28])

1.2 Overview of scalability of skyrmion-mediated voltage-controlled switching of ferromagnets

Recently, the possibility of VCMA-induced magnetization reversal between two ferromagnetic states without any external bias magnetic field has been reported [28]. This is achieved by applying a voltage pulse that reduces PMA. Thus, starting from one of the ferromagnetic states (up/down), an intermediate skyrmion can be created [29-31]. The created skyrmion is a metastable skyrmion and the voltage pulse is withdrawn coincidentally with the breathing motion of the skyrmion. Due

to this, when the initial PMA value is restored, the intermediate skyrmion annihilates to the other [28] ferromagnetic state (down/up). The switching mechanism is shown in Fig. 5.

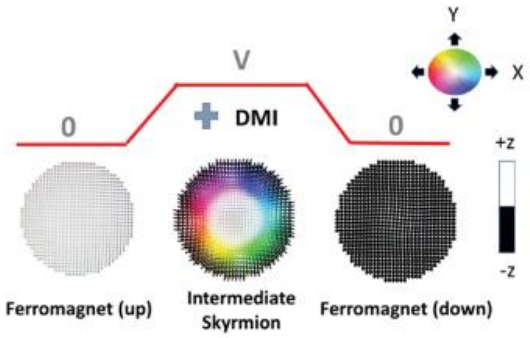

Fig. 5. An energy barrier separates the two nonvolatile states (ferromagnetic up and down states) at equilibrium (V=0). In the presence of DMI in the free layer, a voltage pulse reduces the PMA and a metastable skyrmion is created. By withdrawing the voltage coincidentally with the inbreathing of the skyrmion, the reversal of the ferromagnetic state is achieved. Corresponding states (ferromagnetic up, down, and skyrmion) are shown below the voltage pulse.

Skyrmions are topologically stable [32] particle-like localized spin structures [33-39]. The existence of this outstanding quasi-particle was predicted theoretically [40] and later observed experimentally [41,42,43] in condensed matter systems. Skyrmion can be formed in non-centrosymmetric bulk ferromagnetic materials [42] or at the interface [44-48] of a ferromagnet with a material with large spin orbit coupling due to the existence of Dzyaloshinskii-Moriya interaction [49-52] along with several other competing interactions. Skyrmion has unique topology which can be described in terms of skyrmion number [36] and is given as $s=\frac{1}{4\pi}\int \vec{m}.\left(\frac{\delta\vec{m}}{\delta x}\right)\times\left(\frac{\delta\vec{m}}{\delta y}\right)dx\,dy$, where $\vec{m}$ is the normalized magnetization vector ($\vec{M}/M_s$) and M_s is the saturation magnetization. The skyrmion number tells how many times a sphere can be wrapped with a skyrmion. Depending on the spin rotation from center to periphery, skyrmion can be classified into two types, namely Neel [53, 54] and Bloch skyrmions [55]. The vector field of these two magnetic skyrmion are shown in Fig. 6. DMI vector direction in bulk system prefers Bloch skyrmion whereas interfacial DMI hosts Neel skyrmion.

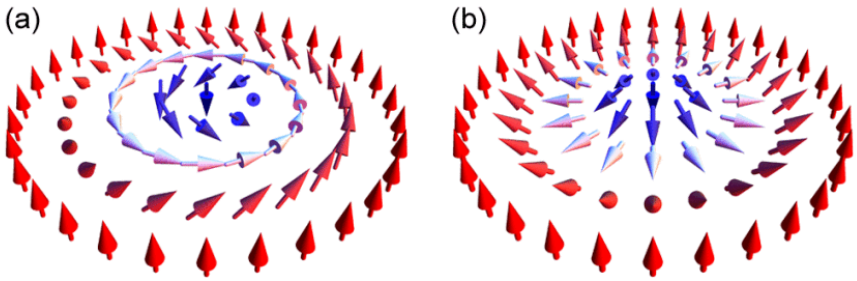

Fig. 6. (a) Bloch skyrmion and (b) Neel skyrmion (Figure is taken from ref [56])

Skyrmions are usually controlled by electrical current in racetrack and was proven to be advantageous, due to its high mobility and potential in overcoming edge roughness-related pinning occurring in domain wall (DW)- based racetrack devices [44, 57-61]. However, the skyrmion mediated switching strategy explored that is illustrated in Fig. 5 uses a confined geometry and, thus, has the potential for higher density memory cells compatible with crossbar architecture. This mechanism has been shown to be robust to thermal noise, disorder and perturbative spin currents for a nanomagnet of lateral dimension 100 nm [28]. However, to be competitive with the current miniaturization trend in STT- magnetic random-access memory (STT-MRAM), further downscaling is required. Chapter 3 theoretically demonstrates the feasibility of downscaling the skyrmion-mediated switching scheme by studying three MTJs of different sizes, 100, 50, and 20 nm, respectively. We show that while skyrmion-mediated switching of ferromagnets in the presence of thermal perturbation is feasible down to lateral dimensions ~20nm, the large values of VCMA and Dzyaloshinskii-Moriya interaction (DMI) needed at ~20nm lateral dimensions have only been theoretically predicted and are yet to be experimentally demonstrated to date.

The findings demonstrated in chapter 3 spurred the investigation on creating and stabilizing skyrmion in scalable nanodots with observable DMI. Previously it has been shown that in multilayer thin ferromagnetic film stacks, skyrmion size can be reduced down to ~50nm starting from several micrometer at room temperature [62,63]. However, due to a large stray field originating from ferromagnetic materials, skyrmion size cannot be further scaled in ferromagnetic thin films [64]. Hence, compensated ferrimagnets have recently emerged as an alternative to ferromagnets for hosting smaller skyrmions due to their small stray fields [65], [66]. In ferrimagnetic thin film of $Co_{44}Gd_{56}$, ~10 nm skyrmion has been observed without any out-of-plane

bias field with lifetime on the order of several minutes [65]. However, in chapter 4, we show that high saturation magnetization favors formation of skyrmions in *confined* (geometrically confined) structures of small lateral dimensions (e.g. nanodots ~20 nm) as opposed to the case of ferrimagnetic thin films where weak stray fields due to low net saturation magnetization helps form smaller skyrmions. We also show that thermally robust skyrmion mediated switching can be attained in a 20 nm nanodot with high saturation magnetization and DMI values ~3mJ/m^2 that have been experimentally observed.

Chapter 2: Micromagnetic modeling of magnetization dynamics

The magnetization dynamics of circular nanodots studied in this thesis work is simulated by using the micromagnetic simulation software Mumax3 [67].

In the Mumax3 software, the magnetization dynamics of the nanodots is simulated by solving the Landau-Lifshitz-Gilbert (LLG) equation:

$$\frac{\partial \vec{m}}{\delta t} = \left(\frac{-\gamma}{1+\alpha^2}\right)\left[\vec{m} \times \vec{B}_{eff} + \alpha\{\vec{m} \times (\vec{m} \times \vec{B}_{eff})\}\right] \quad (1)$$

where α is the Gilbert damping coefficient and γ is the gyromagnetic ratio (rad/Ts). $\vec{m}$ is the normalized magnetization vector ($\vec{M}/M_s$), M_s is the saturation magnetization and $\vec{B}_{eff}$ is the effective magnetic field. The effective magnetic field has the following components:

$$\vec{B}_{eff} = \vec{B}_{demag} + \vec{B}_{exchange} + \vec{B}_{dm} + \vec{B}_{anis} + \vec{B}_{thermal} \quad (2)$$

Here, $\vec{B}_{demag}$ and $\vec{B}_{exchange}$ represent the effective field due to demagnetization energy and the Heisenberg exchange interaction respectively.

Effective field due to Heisenberg exchange interaction can be expressed as:

$$\vec{B}_{exch} = 2\frac{A_{ex}}{M_{sat}}\sum_i \frac{(\vec{m_i} - \vec{m})}{\triangle_i^2}$$

Where *i* is for six nearest neighbors of the central cell with magnetization $\vec{m}$ and $\triangle_i$ is the cell size in the direction of neighbor *i*.

$\vec{B}_{dm}$ indicates the effective field due to the Dzyaloshinskii-Moriya interaction (DMI) which can be expressed as:

$$\vec{B}_{dm} = \frac{2D}{M_s}\left(\frac{\delta m_z}{\partial x}, \frac{\partial m_z}{\delta y}, -\frac{\partial m_x}{\delta x} - \frac{\partial m_y}{\delta y}\right) \quad (3)$$

Where m_x, m_y and m_z are the normalized magnetization components along the three cartesian co-ordinates and D represents the DMI constant (mJ/m^2).

$\vec{B}_{anis}$ is the effective field due to perpendicular anisotropy which is expressed by the following equation:

$$\vec{B}_{anis} = \frac{2K_{u1}}{M_s}(\vec{u}.\vec{m})\vec{u} \tag{4}$$

Here K_{u1} represents first order uniaxial anisotropy constant and $\vec{u}$ indictaes a unit vector in the anisotropy direction. The temperature effect is calculated by:

$$\vec{B}_{thermal} = \vec{\eta}(step)\sqrt{\frac{2\alpha k_B T}{M_s \gamma \Delta V \Delta t}} \tag{5}$$

Where T is the temperature (K), ΔV is the cell volume, k_B is the Boltzmann constant, Δt is time step and $\vec{\eta}(step)$ is a random vector from a standard normal distribution which is independent (uncorrelated) for each of the three cartesian co-ordinates. Its value is changed after every time step.

Chapter 3: Dynamic skyrmion-mediated switching of perpendicular MTJs: Feasibility analysis of scaling to 20 nm with thermal noise

(M. M. Rajib, W. A. Misba, D. Bhattacharya, F. Garcia-Sanchez and J. Atulasimha, IEEE Transactions on Electron Devices, Vol. 67, No. 9, Sept. 2020). Many parts of this paper are verbatim in the thesis chapter.

One method of creating and annihilating skyrmions in confined geometries is to use voltage-controlled magnetic anisotropy (VCMA). The previous study shows that robust voltage-controlled ferromagnetic reversal from "up" to "down" state in the soft layer of a perpendicular magnetic tunnel junction (p-MTJ) can be achieved by creating and subsequently annihilating an intermediate skyrmion state in the presence of room temperature thermal noise and anisotropy variation across grains. However, when scaling to 20 nm, thermal noise can annihilate the skyrmions, for example, by randomly moving the core toward the boundary of the nanostructure. Here, we study three p-MTJs of different dimensions, specifically lateral dimensions of 100, 50, and 20 nm and investigate the change in switching behavior as the dimension is decreased. In particular, we show that while skyrmion-mediated switching of ferromagnets in the presence of thermal perturbation is feasible down to lateral dimensions ~20 nm, the large values of VCMA and Dzyaloshinskii-Moriya interaction (DMI) needed at ~20 nm lateral dimensions have only been theoretically predicted and are yet to be experimentally demonstrated to date.

3.1 Non-thermal study on skyrmion oscillation

Our proposed structure is presented in Fig. 1. The free layers are chosen to be nanodisks of diameters 100, 50, and 20 nm. The thickness-to-diameter ratio (the aspect ratio) is set to 0.012 for 100 and 50 nm MTJs to maintain constant demagnetization factor. However, 0.6 nm thickness is kept unchanged for scaling from a diameter of 50 to 20 nm instead of reducing it to 0.24 nm as such a low thickness would make the device impractical. We consider exchange stiffness A = 25 pJ/m, saturation magnetization $M_s = 1.3 \times 10^6$ A/m, and Gilbert damping coefficient $\alpha = 0.01$. For the successful realization of our switching mechanism, we require an initial ferromagnetic state. Next, when the PMA is reduced (voltage applied), we need to form an intermediate skyrmion state to provide a robust pathway for magnetization reversal to the opposite ferromagnetic state when

the PMA is restored (voltage withdrawn). We vary the perpendicular anisotropy (K_{u1}) and the DMI parameter (D) to fulfill these requirements. The rationale behind choosing different anisotropy and DMI values is discussed below.

TABLE I Material Parameters and Corresponding Energy Barrier

MTJs	K_i ($\mu J/m^2$)	*Energy barrier* (k_BT)	D_{crit} (mJ/m^2)	D (mJ/m^2)
100nm	1332	45.55	1.42	1.2
50nm	1044	51.32	5.25	4.5
20nm	3798	50.09	14.61	13.0

First, to form the intermediate skyrmion state, we need a sizeable DMI. Moreover, the reduction of the lateral dimension requires higher DMI to form an intermediate skyrmion state. However, to maintain an initial ferromagnetic state, the DMI value must be less than the critical value ($D_{crit} = (4/\pi)(AK_{EFF})^{1/2}$, where $K_{EFF} = K_{u1} - (1/2)\,\mu_0\,M_s^2$) at the corresponding initial PMA value. Here, K_{EFF} is the effective perpendicular anisotropy and the D_{crit} (critical DMI) value signifies a threshold beyond which a metastable skyrmion can be formed in the system.

The energy barrier between two ferromagnetic states reduces due to the presence of DMI [68]. To incorporate this reduction, we have estimated the energy barrier with K_{eff} from the phenomenological equation $K_{eff} = (K_{u1} - (1/2)\,\mu_0 M_s^2 - (D^2\pi^2)/(16A))$. The perpendicular anisotropy is determined from the thermal stability factor $K_{eff}V/k_BT$, which is considered to be appropriately around 50 for all three MTJs. Therefore, with a reduction of lateral dimension, required DMI increases, and consequently, the uniaxial anisotropy K_{u1} needs to be increased to ensure thermal stability with an energy barrier of $\sim 50\ k_BT$.

With the reduced thickness of 0.6 nm in cases of 50 and 20 nm along with high PMA, the pinning effect can be presented [69]. However, we do not consider the pinning effect as this is a feasibility study, and including the effect of defects is beyond the scope of this work. Moreover, the stray field from the fixed layer of the MTJ can assist in skyrmion formation [70], [71]. Nevertheless, a small field in either the perpendicular or any of the in-plane directions does not significantly affect

the switching dynamics [28]. Therefore, we do not include stray field in our simulations. The parameters are listed in Table I (A = 25 pJ/m, $M_s = 1.3 \times 10^6$ A/m, and $\alpha = 0.01$ for all cases). We note that the feasibility of the material parameters such as PMA (Ki) and DMI coefficient (D) in Table I (and also the VCMA coefficients are mentioned in Table II) are discussed at the end of this chapter.

First, we study the behavior of the nanomagnets by reducing PMA through VCMA without any thermal perturbation. At reduced PMA, the competing PMA, DMI, and demagnetization form a skyrmion. Once the skyrmion is formed, it starts to oscillate between two stable states: skyrmionic state and quasi-ferromagnetic state. The oscillation is observed in the form of topological charge evolution with time (see Fig. 7) where the crests indicate a skyrmionic state and troughs indicate a quasi-ferromagnetic state. With the reduction of the lateral dimension, the DMI required to form an intermediate skyrmion state increases. Thus, it forces the magnetization to oscillate at a higher frequency. This reduces the pulsewidth and the rise time of the voltage pulse applied that can produce favorable switching in the smaller nanomagnets. VCMA coefficients, fall and rise time, total change in PMA, oscillation frequency, and pulsewidth range are listed in Table II considering the application of voltage pulse (ΔV) of 2.0 V across 1-nm-thick MgO layer for all three MTJs.

By withdrawing the voltage pulse and restoring the PMA to the initial values at each peak point, switching is observed. When PMA is restored, the intermediate skyrmions are collapsed and go to either the opposite ferromagnetic state or back to the initial ferromagnetic state due to the minimization of curvature energy ($\sigma = 4(AK_{EFF})^{1/2} - \pi D$) of the 360◦ DW of the skyrmion's spin spiral [72]. In addition to this, we exploit in breathing dynamics to ensure the resulting ferromagnetic state is opposite to the initial state resulting in the skyrmion mediated reversal. Fig. 7 shows that the nanomagnets switch for the first 5, 5, and 7 cycles, respectively, for 100-, 50-, and 20-nm lateral dimension (diameter) nanomagnets. Beyond these cycles (for respective nanomagnet sizes), the topological number falls below the critical value and therefore an intermediate skyrmion state is not available for successful switching. The "switch" and "no switch" regions along with the comparison of topological evolution for three nanomagnets are shown in Fig. 7. By the "switch" region, we mean that when the voltage pulse is withdrawn (PMA restored) roughly at the maxima of the topological charge in Fig. 7, the magnetization of the nanomagnet relaxes to a ferromagnetic state that is opposite (reversed) from the original state. In

other words, the switching or reversal is successful. In the "no switch" region, even if the voltage pulse is withdrawn (PMA restored) roughly at the maxima of topological charge the magnetization relaxes to the original ferromagnetic state and thus does not switch successfully.

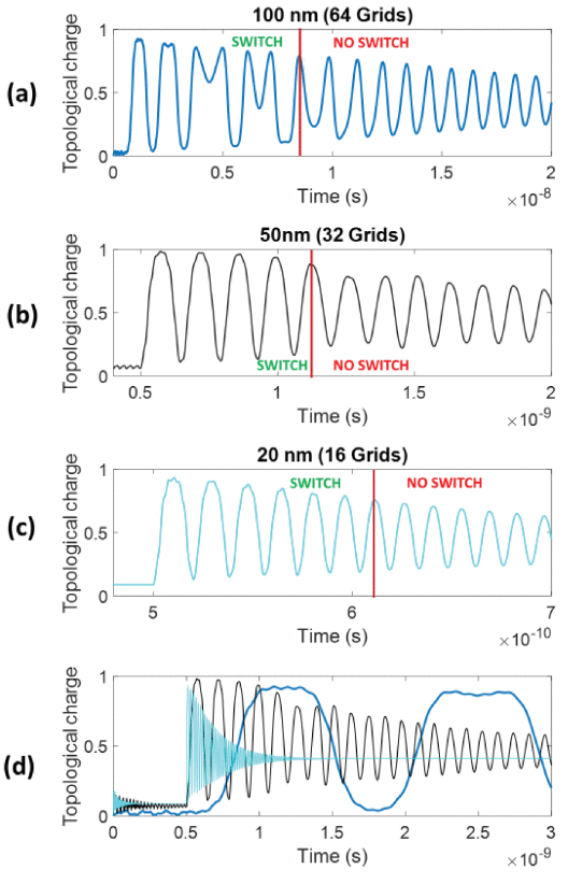

Fig. 7. "Switch" and "no switch" regions without thermal perturbation for (a) 100, (b) 50, (c) 20 nm. (d) Comparison of topological evolution of three nanomagnets using the same time scale for the nanomagnets of three different sizes.

TABLE II Columns 2–4 are parameters chosen and columns 5 and 6 are inferred from simulations

MTJs	VCMA Coeff. (fJ/Vm)	Fall/ rise time (ps)	ΔK_i ($\mu J/m^2$)	*Pulse-width range (ps)*	*Osc. Freq. (GHz)*
100nm	102	100	204	*500-900*	*~1*
50nm	252	1	504	*22-102*	*~8*
20nm	1569	0.5	3138	*4-13*	*~60*

3.2 Thermal switching

In the presence of room temperature thermal noise, the first breathing period of a skyrmion is ideal for the switching to minimize the possibility of intermediate skyrmion annihilation due to thermal noise. The switching percentage for 100-nm nanomagnet with pulsewidth range of 400–700 ps is studied and shows thermally robust switching in the 450–650 ps range [see Fig. 8(a)]. For 50 nm, thermally robust switching is observed for the pulsewidth range of 32–42 ps by studying the switching percentage in the pulsewidth range of 22–102 ps [see Fig. 8(b)]. For 20 nm, the switching percentage is studied for pulsewidth range of 4–13 ps. Within this range, 99% switching is observed in the pulsewidth range of 6–7 ps [see Fig. 8(c)].

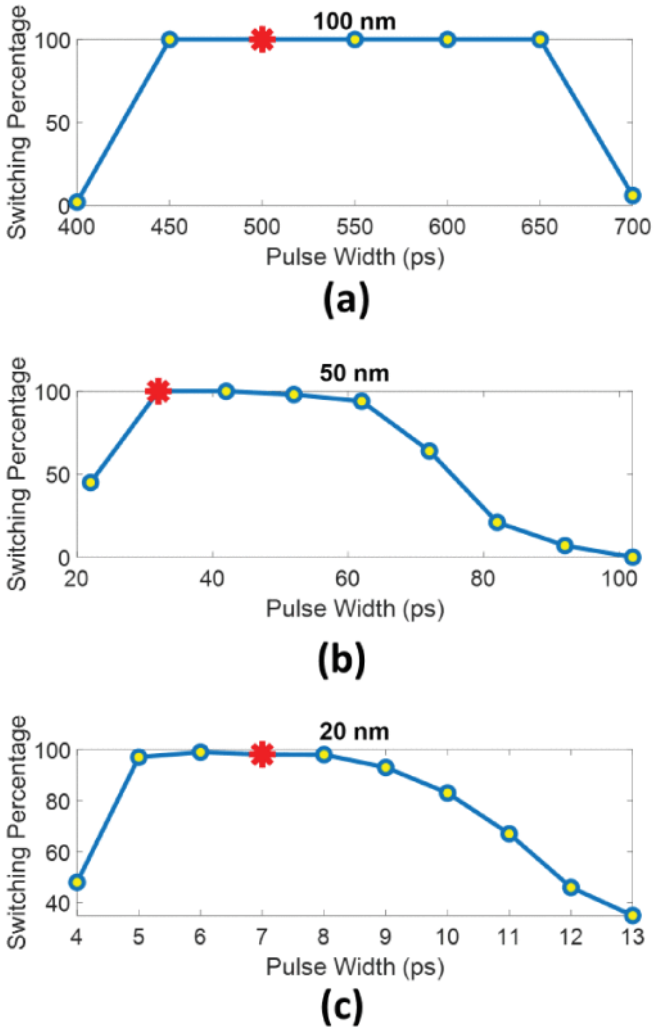

Fig. 8. Switching probability versus pulsewidth of (a) 100, (b) 50, and (c) 20 nm nanomagnets. [For studying the switching percentage for different pulsewidths, the simulations were run for 100 times for

most points. For one point in each subfigure, the simulations were run 1000 times. Thus, points marked as 100% with a star (indicate a better than 99.9% switch for 100- and 50-nm lateral dimensions as there is no failure for 1000 runs). However, for a 20-nm case, 19 failures in 1000 runs at pulsewidth of 7 ps indicate ~98% switching.]

3.3 Switching energy per bit:

Considering an application of a voltage pulse of 2.0 V for a 1.2-nm-thick free layer and a 1-nm-thick MgO layer with relative permittivity of ~7, energy dissipated per switching event in a 100-nm nanomagnet is ~1 fJ. Sub 1 fJ/bit switching for 20-nm nanomagnet can be achieved (provided large VCMA coefficient, PMA, and DMI are available) which is highly desirable for energy efficient memory devices.

In summary, our simulations show that thermally robust switching with a frequency of 2 GHz can be attained for a 100 nm nanomagnet. This switching remains robust when scaling down to 50 nm lateral dimensions in the presence of thermal noise with a switching frequency of ~20 GHz with appropriate choice of feasible material parameters based on experimentally reported values of VCMA coefficient (370 fJ/Vm) [73], PMA (3700 μJ/m^2) [74] and DMI (~3mJ/m^2) [75,76,77].

Similarly, while downscaling to 20 nm, thermally robust switching with a very large frequency in the range of ~100 GHz can be achieved provided material parameters with large VCMA [78], DMI [79, 80] and PMA [74, 78] are chosen. Among these three parameters only PMA [74] has been experimentally reported, while DMI and VCMA values (for the 20 nm nanomagnet simulation) have only been theoretically predicted [78,79,80] to date but not experimentally demonstrated. This is an important challenge in scaling from 50 to 20 nm.

Chapter 4: Robust skyrmion mediated reversal of ferromagnetic nanodots of 20 nm lateral dimension with high M_s and observable DMI

(M. M. Rajib, W. A. Misba, D. Bhattacharya, and J. Atulasimha, https://doi.org/10.1038/s41598-021-99780-1) Many parts of this paper are verbatim in the thesis chapter.

Implementation of skyrmion based energy efficient and high-density data storage devices requires aggressive scaling of skyrmion size. Ferrimagnetic materials are considered to be a suitable platform for this purpose due to their low saturation magnetization (i.e. smaller stray field). However, this method of lowering the saturation magnetization and scaling the lateral size of skyrmions is only applicable where the skyrmions have a smaller volumetric ratio compared to lateral dimensions of the hosting film. In this chapter, we show by performing rigorous micromagnetic simulation that the size of skyrmions which have lateral dimension comparable to their hosting nanodot can be scaled by increasing saturation magnetization. Also, when the lateral dimension of nanodot is squeezed and thereby the skyrmion confined in it is downscaled there remains a challenge in forming stable skyrmion with observable Dzyaloshinskii-Moriya interaction (DMI) since this interaction has to facilitate higher rotation per spin to complete a 360^0 along the diameter. In our study, we found that skyrmions can be formed in 20 nm lateral dimension nanodots with high saturation magnetization (1.30-1.70 MA/m) and observable DMI (~3 mJ/m^2). This result could stimulate experiments on implementation of highly dense skyrmion devices. Additionally, using this, we show that Voltage Controlled Magnetic Anisotropy (VCMA) based switching mediated by an intermediate skyrmion state can be achieved in the soft layer of a ferromagnetic p-MTJ of lateral dimensions 20 nm with sub 1fJ/bit energy in the presence of room temperature thermal noise with reasonable DMI ~3 mJ/m^2.

4.1 Stabilization of skyrmions in smaller nanodots with higher M_s and DMI

To study the formation of stable skyrmion we simulated the magnetization dynamics of circular nanodots of 50 nm, 30 nm and 20 nm lateral dimensions using the micromagnetic simulation software Mumax3 [67]. In all three cases, we initiate the simulations from a purely ferromagnetic state (all the spins pointing in the +z direction) and relax for 1 ns, which ends up a quasi-ferromagnet (QFM) as shown in Fig. 9. We can see that in QFM the boundary spins are slightly

tilted. The perpendicular magnetic anisotropy (PMA) is then reduced through VCMA in 0.5 ps. It is noteworthy that achievement of smaller ramp time requires smaller RC constant which in turn depends on the availability of smaller resistance area product (RA). Considering 1nm thick MgO layer, the required RA product (~8 $\Omega.\mu m^2$) for achieving such small ramp time is within the experimentally reported values [81, 82]. After 3ns the voltage pulse is withdrawn and the PMA is restored to the initial value. We see the equilibrium state after 5ns and observe that the final state is either a QFM or skyrmion. We find that after the withdrawal of voltage pulse, 5 ns is sufficient for reaching a stable state. This was confirmed by studying one equilibrium state (M_s=1650kA/m, DMI=3.2 mJ/m^2) for 1 μs and there was no change in average out-of-plane magnetization component or topological charge from those obtained after 5ns. To find the required saturation magnetization (M_s) and DMI as the lateral dimension of the nanodot is varied, the initial and reduced effective perpendicular anisotropy energy along with other parameters listed in Table III are kept constant. The effective PMA energy is expressed as $K_{eff}V = \left(K_{u1} - \frac{1}{2}\mu_0 M_s^2\right)V$, where K_{u1} is the PMA constant (uniaxial anisotropy) and V is the volume of the nanodot. The saturation magnetization is varied from 700 kA/m to 1700 kA/m for all nanodots.

Table III: List of parameters

Exchange stiffness	5 pJ/m
Thickness	0.6 nm
Gilbert damping coefficient	0.05
Cell size	0.5nm×0.5nm×0.6nm
Initial effective PMA energy	50 kT
Reduced effective PMA energy	2.73 kT

The stable state turns out to be either a QFM or a skyrmion state. Figure 9 shows an example case of formation of a stable skyrmion in 20nm nanodot through VCMA where M_s=1650 kA/m and DMI=3.2mJ/m^2. The skyrmion is created when the effective PMA energy is reduced and remains stable even after the restoration of effective PMA energy to the initial value by withdrawing the voltage pulse. The initial PMA value plays a critical role in determining the final state. If the initial effective PMA energy is bigger than a critical effective anisotropy energy, QFM state is observed. For 20 nm nanodot we observe this critical initial effective PMA energy is ~64kT at DMI ~3mJ/m^2.

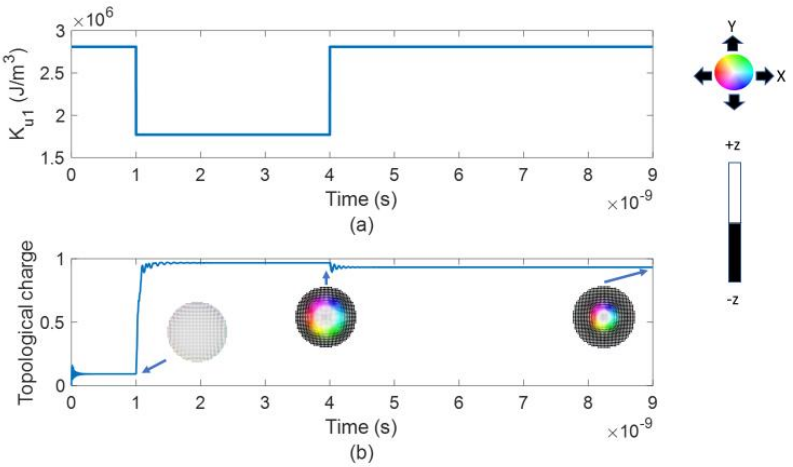

Fig. 9. (a) Application of VCMA, (b) A quasi-ferromagnetic (QFM) state is created after relaxing for 1ns. After the reduction of PMA, a skyrmion is formed and it is stable even after the withdrawal of voltage pulse.

By following the strategy illustrated in Fig. 9(a) we calculate the required M_s and DMI values for which skyrmions are formed in 20nm, 30nm and 50nm nanodots. This is shown by D-M_s phase diagrams in Fig. 10.

It is understandable that in 20nm nanodot there will be higher rotation per spin and the requirement of DMI will be higher compared to 30nm and 50nm nanodot for a constant effective PMA energy. In chapter 3, it has been shown that even for formation of transient skyrmion, an extremely large DMI is required. So, it becomes a challenge to create a skyrmion in a 20 nm nanodot with experimentally observed DMI. Therefore, we focus on exploring the minimum DMI under a constant effective PMA energy while the DMI is within the observable limit. We also observe the saturation magnetization associated with the minimum DMI needed to explore which minimum DMI and M_s combination helps stabilize skyrmions in nanodots. In addition to that, we explore some other DMI values close to the minimum DMI range and observe the corresponding M_s values for the formation of skyrmion as shown in Fig. 10.

Figure 10(a) shows the D-M_s phase diagram for a 20nm nanodot. We can see that minimum DMI for creating a stable skyrmion with a constant effective PMA energy as mentioned in Table III is 2.95mJ/m^2. Saturation magnetization required to form the skyrmion at this DMI value is 1300-1350 kA/m. Below 2.95 mJ/m^2 DMI, no skyrmion is formed. As the DMI value is increased the M_s range for which skyrmion can be created becomes wider at the higher M_s values. Considering

a 1nm thick MgO layer and an application of a voltage pulse of 2.0 V, the VCMA coefficient required to form these skyrmions in a 20nm nanodot is 312 fJ/Vm.

We next increased the lateral dimension to 30 nm and explored the minimum DMI required to form skyrmions in the 700-1700 kA/m M_s range at the effective PMA energy equal to that of 20nm. From Fig. 10(b) we can see that the minimum DMI required for the formation of skyrmions in a 30 nm nanodot is 1.95 mJ/m^2 and the M_s range is 1000-1050 kA/m. At higher DMI, the M_s range for which the skyrmion is created grows wider similar to the 20nm case.

The D-M_s relation required for formation of stable skyrmion in increased lateral dimension to 50nm is shown by Fig. 10(c). Minimum DMI required for the formation of stable skyrmion is 1.15mJ/m^2 and corresponding M_s value is 750kA/m. Considering the MgO layer thickness and application of voltage pulse the same as 20nm, VCMA coefficient for skyrmion formation in 30nm and 50nm nanodot are 139 fJ/Vm and 50fJ/Vm respectively.

For 50nm, though a skyrmion is observed for a minimum DMI value of 1.15mJ/m^2 and M_s value of 750 kA/m but no skyrmion is found for the same DMI and higher M_s. For other DMI values close to the minimum DMI, the required M_s remains still in the comparatively lower range of M_s values. For 20nm, the minimum DMI happens at higher M_s value and for other DMI values close to the minimum DMI, the required M_s values are also in higher range. Expectedly, minimum DMI and M_s values for 30 nm fall in between those values required for 20nm and 50nm. Since the minimum DMI is associated with high M_s values in 20nm nanodot, we can say that large saturation magnetization helps stabilize skyrmion in smaller nanodots. This trend of downscaling of skyrmion lateral dimension draws a significant contrast with the downscaling of skyrmion size in thin films. In thin film, lowering the saturation magnetization helps form smaller skyrmion whereas in nanodot high saturation magnetization is helping stabilize smaller skyrmions.

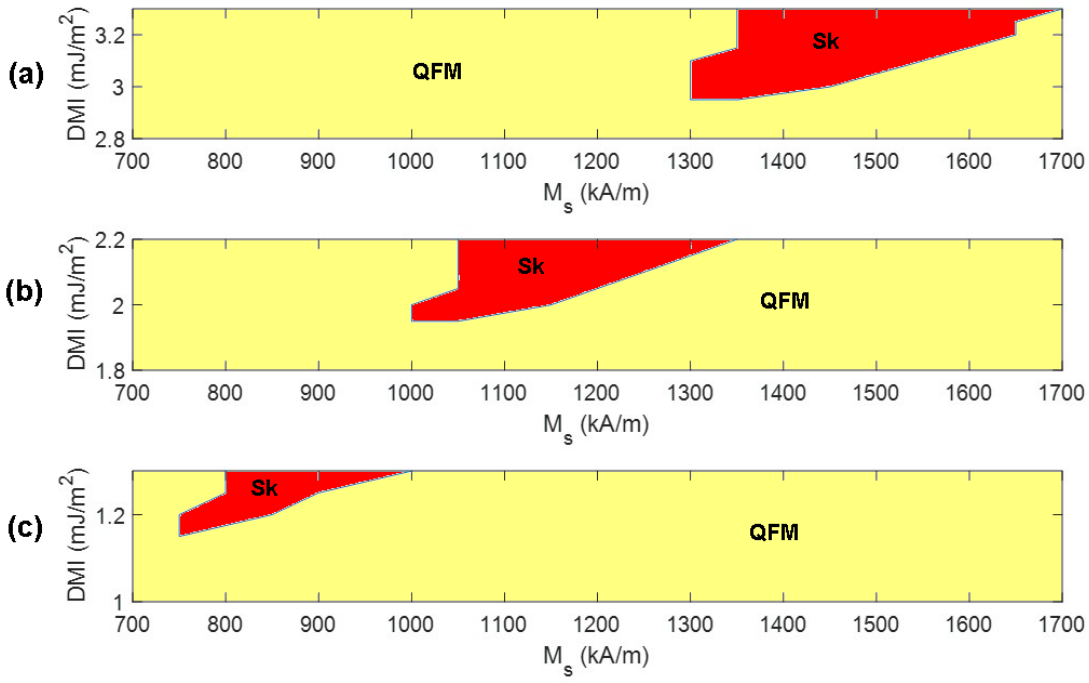

Fig. 10. D-M_s phase diagram for (a) 20 nm, (b) 30nm and (c) 50nm (QFM and Sk in the phase diagrams represent the regions where these states are observed)

To study how the skyrmions are formed at high M_s in downscaled nanodots, we observe the total energy of the equilibrium states for 20nm nanodot for various M_s values. We take two M_s values, one from the higher end (1650kA/m) and the other from lower end (1000kA/m) of M_s range at a constant DMI (3.2mJ/m^2) and observed the dynamic evolution of the magnetic states and their corresponding energy as shown in Fig. 11. For 1000 kA/m, skyrmion forms after 25 ps when PMA is reduced. The breathing of skyrmion is very fast and annihilates after ~100 ps. After the annihilation of skyrmions, the nanodot stabilizes at QFM state. For 1650kA/m, skyrmion forms slowly, specifically at ~100 ps after the PMA is reduced. The skyrmion formed in this case also breathes slowly and stabilizes at this state.

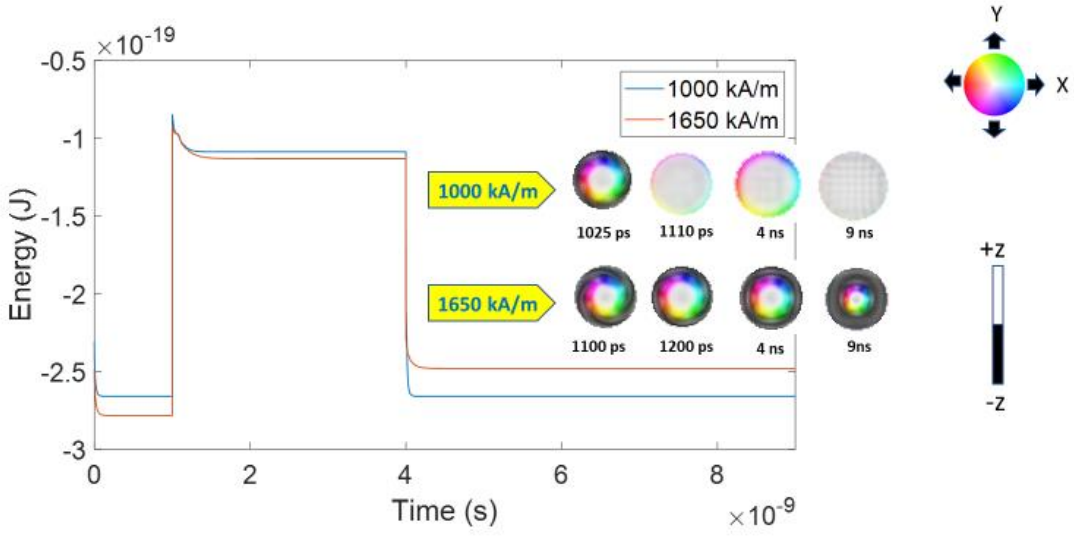

Fig. 11. Evolution of total energy for two different M_s values and their corresponding magnetic states at different times.

The requirement of higher DMI for decreased dimension of nanodots can be explained as follows. A higher DMI strength is required for completing the 360-degree rotation along a smaller diameter. Furthermore, when DMI is kept at the minimum required, high M_s is needed as it helps the formation of stray field dominated skyrmions in the confined nanostructure. Figure 12 shows that for 20 nm nanodots and 3.2 mJ/m^2 DMI, minimum M_s at which a skyrmion is formed is 1350 kA/m whereas minimum M_s for the formation of skyrmion at 4.0 mJ/m^2 DMI is only 700 kA/m. In summary, high M_s is not needed if we could employ high DMI and therefore form DMI mediated skyrmions. On the other hand, using low DMI requires a high M_s so that the stray field can aid the DMI in formation and stabilization of the skyrmions.

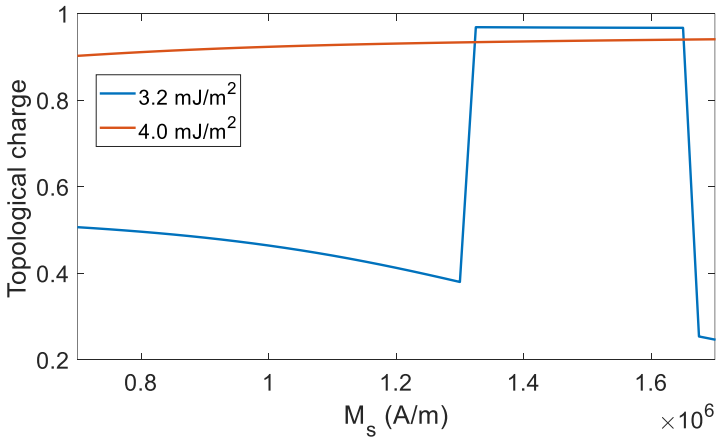

Fig. 12. Topological charge vs. saturation magnetization of 20 nm nanodot for 3.2 mJ/m^2 and 4.0 mJ/m^2 DMI.

4.2 **Skyrmion-mediated voltage controlled switching of ~20nm nanodot (with inclusion of room temperature thermal noise)**

In this section, we study the switching probability of 20 nm lateral dimension ferromagnetic nanodot by employing VCMA induced skyrmion mediated switching. In such switching, in chapter 3 as we have discussed, an intermediate skyrmion is created starting from a ferromagnetic state by lowering PMA which is subsequently annihilated by restoring the PMA to achieve switching from ferromagnetic up/down to down/up state. This reversal mechanism is implemented in a similar way that is followed for stabilizing skyrmion but the only difference is in the timing of withdrawal of voltage pulse. In stabilization, voltage pulse is withdrawn after the skyrmion has been stabilized after some initial breathing at reduced PMA whereas in reversal the voltage pulse is withdrawn while the skyrmion breathes. From the non-thermal stabilization, we have seen that for both cases of $M_{s,}$ primarily a skyrmion is formed but for lower value of M_s the breathing is very fast and it cannot be stabilized. Though for skyrmion mediated magnetization reversal only a transient skyrmion is required but stabilization gives an idea where skyrmion breathes slowly, survives longer and provides potential robust switching.

For non-thermal stabilization of skyrmions, the stability factor ($K_{eff}V/k_BT$) at reduced PMA is ~ 2.73. So, the thickness of the 20nm nanodot is increased from 0.6nm to 1.5nm, keeping the reduced effective PMA energy density constant (60,000 J/m^3) similar to non-thermal cases, to make the transient skyrmion thermally stable. Also, there is a critical value of initial PMA below which intermediate skyrmion cannot be annihilated after the withdrawal of voltage pulse as discussed in the non-thermal stabilization. Therefore, the initial PMA is increased for studying reversal at room temperature in the presence of thermal perturbation. For studying the switching probability, we take two M_s values, 1000kA/m and 1650 kA/m at a constant DMI 3.2mJ/m^2. The initial and reduced effective PMA energy are 330kT and 6.83kT respectively for both 1000kA/m and 1650kA/m system. Therefore, the initial and reduced interfacial magnetic anisotropy (K_i) for 1650kA/m are 6900μJ/m^2 and 2700μJ/m^2 whereas the corresponding values for 1000kA/m are 5300μJ/m^2 and 1000μJ/m^2 respectively. From non-thermal stabilization we observed that for both values of M_s, initially a skyrmion is formed but for low value of M_s (1000kA/m) this skyrmion

does not stabilize. Since in reversal a transient skyrmion is enough so both low and high values of M_s are supposed to provide reversal if the voltage pulse is withdrawn coherently with the breathing of skyrmion. Therefore, we consider these two values of M_s to study which M_s value favors the thermally robust switching more. We let both systems relax for 100 ps to get the equilibrium state before trying to switch the magnetization. Due to the large PMA, this state is very close to the ferromagnet state with very small canting of peripheral spins due to stray field. After relaxing, we apply VCMA to reduce the PMA within 0.5 ps and a skyrmion is formed. We then restore the PMA by withdrawing the voltage pulse at different points (times in formation and dynamics of the skyrmion state) and observe switching. In this switching event, sub 1 fJ energy is dissipated on application of a voltage pulse of 2.0 V with 2130 fJ/Vm VCMA coefficient for a 1.5-nm-thick free layer and a 1-nm-thick MgO layer with relative permittivity ~7. We note that a high VCMA coefficient is needed as we chose a high initial PMA to ensure $K_{eff}V/k_BT\sim 330$. If we go with a smaller $K_{eff}V/k_BT\sim 65$, which suffices for Random Access Memory (RAM), an interfacial PMA energy ~3500μJ/m^2 and VCMA coefficient ~405fJ/Vm would be sufficient for 1650kA/m M_s system. We also note that for $K_{eff}V/k_BT\sim 65$, those required values would be well within the experimentally demonstrated values of interfacial PMA energy ~4060μJ/m^2 [83] and VCMA coefficient ~1043fJ/Vm [84]. From Fig. 13(b) we can see that for a pulsewidth range of 47ps-107 ps, highest switching percentage for 1000 kA/m is 81 at 47ps pulsewidth whereas for 1650 kA/m M_s, ~93% switching can be achieved in 57-77 ps pulse width range. For both stabilization and thermal reversal of skyrmions, it appears that the boundary spins initiate the process of skyrmion formation where the edges of the circular nanodot are nearly smooth. So, we studied this system's behavior in a nanodot where edge roughness is present. Therefore, we incorporated 5% edge roughness as shown in Fig. 13(b) at the boundary of the 20 nm nanodot to study the switching error in the same pulse width range of 47-107ps. We note that the 5% edge roughness was created using a Gaussian distribution. From Fig. 13(c) we can see that in the presence of edge roughness for 1650 kA/m M_s and 3.2 mJ/m^2 DMI, ~80% switching can be attained in the pulse width range of 47-57ps. With better optimization of the material parameters (e.g. high M_s and experimentally observed DMI) and pulse shaping [85] which is beyond the scope of this paper, higher switching percentage can be attained with sub fJ energy for each switching event. For example, the point in Fig. 13(c) with asterisk represents 93% switching at a pulse width of 67 ps.

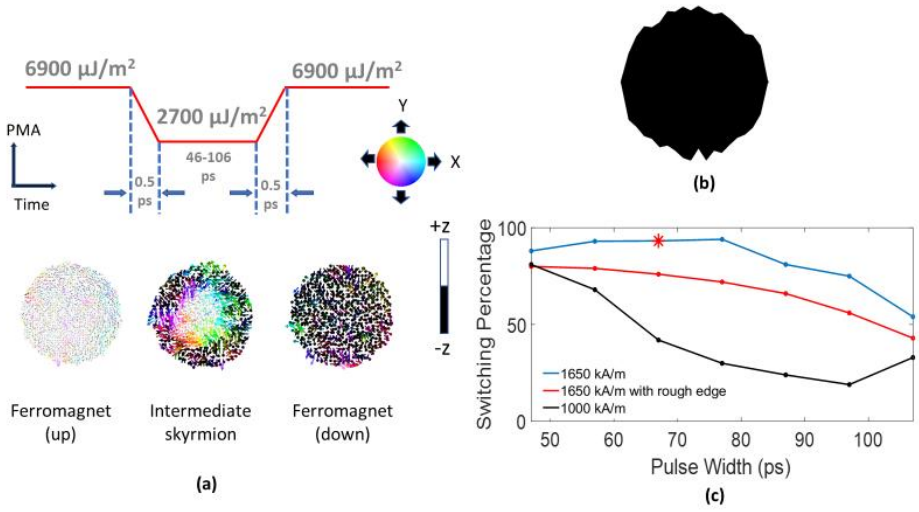

Fig. 13. (a) Voltage pulse described in terms of PMA for switching of 20 nm nanodot in the presence of thermal perturbation; magnetization states corresponding to the PMA energy at different times are shown below the pulse diagram (b) 20nm nanodot with 5% edge roughness at the boundary and (c) Switching percentage vs. pulse width (all of the points show the switching percentage for 100 simulation cases except the point marked with asterisk on the blue line. The star mark corresponds to 67 ps pulse width where the simulations were run for 1000 times and 68 failures indicate ~93% switching).

In summary, higher DMI can result in formation of skyrmions in smaller nanodots at low M_s but such high values of DMI have not yet been experimentally observed. To create skyrmions in confined structures ~20 nm lateral dimensions with experimentally observed DMI ~3 mJ/m^2, one needs large demagnetization (stray field) from materials that can be achieved with a high M_s. We also showed that using a material with high saturation magnetization can help achieve thermally robust and extremely energy efficient switching in 20 nm ferromagnetic nanodot with experimentally demonstrated DMI. Thus, use of materials with high M_s can provide a pathway for aggressive scaling of ferromagnetic skyrmion mediated VCMA switching of p-MTJs with lateral dimensions ~20 nm and beyond.

Chapter 5: Future works

I'll be working on the following projects as a continuation of my present research works towards PhD degree:

Previously our group experimentally showed the manipulation of fixed magnetic skyrmions with voltage-controlled magnetic anisotropy [31]. It was observed that due to the presence of exchange bias field in antiferromagnet/ferromagnet/oxide heterostructure, skyrmions could be stabilized in those thin films. Additionally, due to application of positive (negative) voltage, the PMA decreases (increases) which in effect creates (annihilates) skyrmion in the thin film as shown in Fig. 14. However, the voltage pulse was applied outside of the characterization tool and the transformation was observed in the absence of applied electric field.

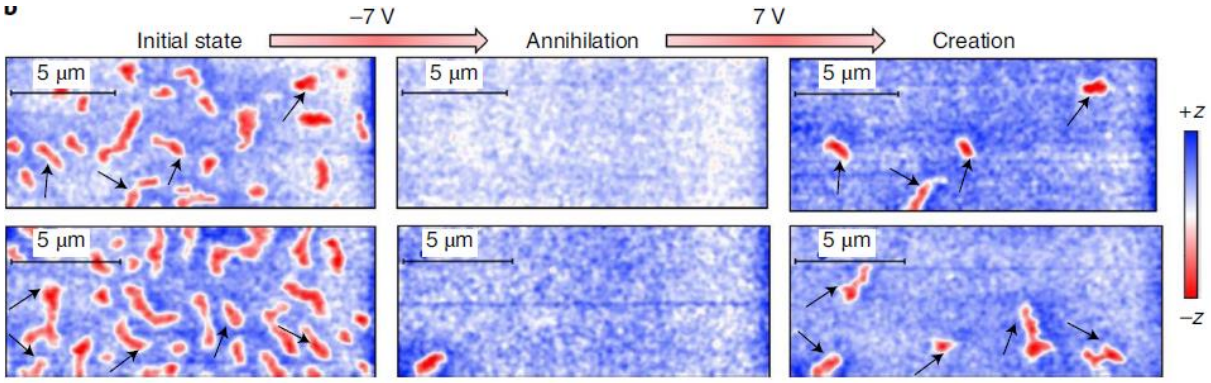

Fig. 14. Magnetic force microscopy (MFM) images taken before and after application of the electric field. First column: MFM image taken before the application of electric field. Second column: A negative voltage pulse increased the PMA and skyrmions were annihilated. Third column: positive voltage pulse decreased the PMA and skyrmions were created. Black arrows indicate that skyrmions created by VCMA appear at the same initial location they occupied before annihilation. (Figure is taken from ref [31])

In future, we will be focusing on in-situ application of VCMA and observing the creation and annihilation of skyrmion in confined geometry while performing MFM.

5.1 Experimental observation of skyrmion-mediated switching in a confined geometry: towards skyrmion mediated memory.

In chapter 3 and 4 we have discussed the skyrmion-mediated reversal of p-MTJs in a confined nanodot. The formation of a transient skyrmion is needed for successful implementation of this theoretically predicted switching strategy. However, experimental creation and annihilation of non-volatile fixed magnetic skyrmions using VCMA has only been realized in thin films in the absence of applied electric filed due to inhomogeneities and defects rather than geometric boundary conditions. In future, we plan to apply VCMA in-situ in a confined geometry and study the dynamic formation and annihilation of skyrmion in proof of concept nanostructures ~100 nm lateral dimensions as well as study skyrmion mediated switching (reversal) of magnetization in perpendicular nanomagnets. This will form a proof-of-concept scalable robust and energy efficient skyrmion mediated p-MTJ switching paradigm.

5.2 Skyrmion based reservoir computing

The recurrent neural network of a reservoir computing system can be imitated by the internal dynamics of a physical system [86, 87, 88, 89, 90]. We use a thin film hosting multiple skyrmions as shown in Fig. 15 and exploit its nonlinear dynamics in response to an applied electric field and coupling through dipole interaction and spin waves for performing simple temporal pattern recognition and time-series prediction tasks.

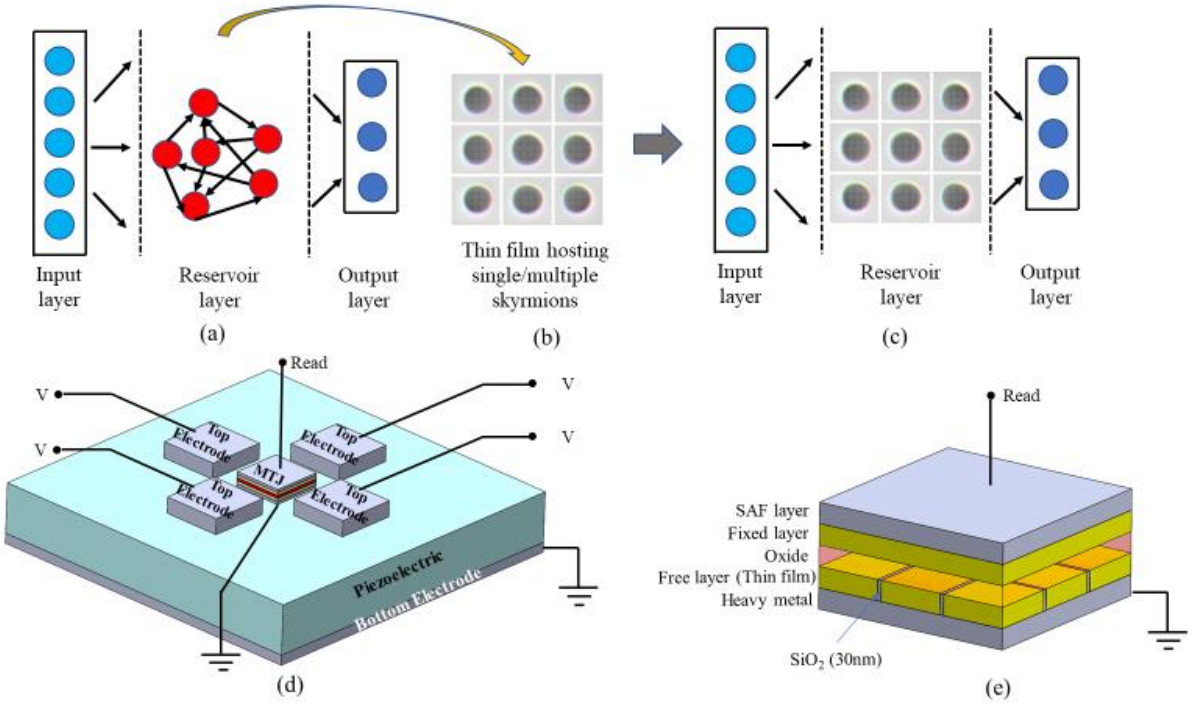

Fig. 15. (a) Schematic illustration of a reservoir computer based on a recurrent neural network (RNN), (b) Thin film hosting skyrmions serves as a reservoir block (skyrmions are represented by the circular dots in the thin film), (c) A skyrmion based physical reservoir computing system obtained by replacing the recurrent network of (a) by the skyrmion-hosting thin film. (d) In the proposed device the free layer of the magnetic tunnel junction (MTJ) acts as the reservoir block. Voltage generated strain is provided as an input to the reservoir layer and the MTJ readout is used for reservoir computing output. (e) Different layers of MTJ stack. (Figure is taken from ref [91])

References

[1] Moore G. E., 1965. Cramming more components onto integrated circuits. Electronics magazine, p. 4.

[2] Valet, T. and Fert, A.J.P.R.B., 1993. Theory of the perpendicular magnetoresistance in magnetic multilayers. *Physical Review B*, *48*(10), p.7099.

[3] Julliere, M., 1975. Tunneling between ferromagnetic films. *Physics letters A*, *54*(3), pp.225-226.

[4] Miyazaki, T. and Tezuka, N., 1995. Giant magnetic tunneling effect in Fe/Al2O3/Fe junction. *Journal of magnetism and magnetic materials*, *139*(3), pp.L231-L234.

[5] Moodera, J.S., Kinder, L.R., Wong, T.M. and Meservey, R., 1995. Large magnetoresistance at room temperature in ferromagnetic thin film tunnel junctions. *Physical review letters*, *74*(16), p.3273.

[6] Parkin, S.S.P., 1995. Giant magnetoresistance in magnetic nanostructures. *Annual review of materials science*, *25*(1), pp.357-388.

[7] Butler, W.H., Zhang, X.G., Schulthess, T.C. and MacLaren, J.M., 2001. Spin-dependent tunneling conductance of Fe| MgO| Fe sandwiches. Physical Review B, 63(5), p.054416.

[8] Mathon, J. and Umerski, A., 2001. Theory of tunneling magnetoresistance of an epitaxial Fe/MgO/Fe (001) junction. Physical Review B, 63(22), p.220403.

[9] Yuasa, S., Nagahama, T., Fukushima, A., Suzuki, Y. and Ando, K., 2004. Giant room-temperature magnetoresistance in single-crystal Fe/MgO/Fe magnetic tunnel junctions. Nature materials, 3(12), pp.868-871.

[10] Ikeda, S., Hayakawa, J., Ashizawa, Y., Lee, Y.M., Miura, K., Hasegawa, H., Tsunoda, M., Matsukura, F. and Ohno, H., 2008. Tunnel magnetoresistance of 604% at 300 K by suppression of Ta diffusion in Co Fe B⁄ Mg O⁄ Co Fe B pseudo-spin-valves annealed at high temperature. Applied Physics Letters, 93(8), p.082508.

[11] Slonczewski, J.C., 1996. Current-driven excitation of magnetic multilayers. *Journal of Magnetism and Magnetic Materials*, *159*(1-2), pp.L1-L7.

[12] Berger, L., 1996. Emission of spin waves by a magnetic multilayer traversed by a current. *Physical Review B*, *54*(13), p.9353.

[13] Sun, J.Z., 1999. Current-driven magnetic switching in manganite trilayer junctions. *Journal of Magnetism and Magnetic Materials*, *202*(1), pp.157-162.

[14] Katine, J.A., Albert, F.J., Buhrman, R.A., Myers, E.B. and Ralph, D.C., 2000. Current-driven magnetization reversal and spin-wave excitations in Co/Cu/Co pillars. *Physical review letters*, *84*(14), p.3149.

[15] Kubota, H., Fukushima, A., Yakushiji, K., Nagahama, T., Yuasa, S., Ando, K., Maehara, H., Nagamine, Y., Tsunekawa, K., Djayaprawira, D.D. and Watanabe, N., 2008. Quantitative measurement of voltage dependence of spin-transfer torque in MgO-based magnetic tunnel junctions. *Nature Physics*, *4*(1), pp.37-41.

[16] Shiota, Y., Nozaki, T., Bonell, F., Murakami, S., Shinjo, T. and Suzuki, Y., 2012. Induction of coherent magnetization switching in a few atomic layers of FeCo using voltage pulses. *Nature materials*, *11*(1), pp.39-43.

[17] Amiri, P.K. and Wang, K.L., 2012, September. Voltage-controlled magnetic anisotropy in spintronic devices. In *Spin* (Vol. 2, No. 03, p. 1240002). World Scientific Publishing Company.

[18] Wang, W.G., Li, M., Hageman, S. and Chien, C.L., 2012. Electric-field-assisted switching in magnetic tunnel junctions. *Nature materials*, *11*(1), pp.64-68.

[19] Maruyama, T., Shiota, Y., Nozaki, T., Ohta, K., Toda, N., Mizuguchi, M., Tulapurkar, A.A., Shinjo, T., Shiraishi, M., Mizukami, S. and Ando, Y., 2009. Large voltage-induced magnetic anisotropy change in a few atomic layers of iron. *Nature nanotechnology*, *4*(3), pp.158-161.

[20] Grezes, C., Ebrahimi, F., Alzate, J.G., Cai, X., Katine, J.A., Langer, J., Ocker, B., Khalili Amiri, P. and Wang, K.L., 2016. Ultra-low switching energy and scaling in electric-field-controlled nanoscale magnetic tunnel junctions with high resistance-area product. *Applied Physics Letters*, *108*(1), p.012403.

[21] Kang, W., Ran, Y., Zhang, Y., Lv, W. and Zhao, W., 2017. Modeling and exploration of the voltage-controlled magnetic anisotropy effect for the next-generation low-power and high-speed MRAM applications. *IEEE Transactions on Nanotechnology*, *16*(3), pp.387-395.

[22] Tiercelin, N., Dusch, Y., Preobrazhensky, V. and Pernod, P., 2011. Magnetoelectric memory using orthogonal magnetization states and magnetoelastic switching. *Journal of Applied Physics*, *109*(7), p.07D726.

[23] Cui, J., Hockel, J.L., Nordeen, P.K., Pisani, D.M., Liang, C.Y., Carman, G.P. and Lynch, C.S., 2013. A method to control magnetism in individual strain-mediated magnetoelectric islands. *Applied Physics Letters*, *103*(23), p.232905.

[24] Nowak, J.J., Robertazzi, R.P., Sun, J.Z., Hu, G., Park, J.H., Lee, J., Annunziata, A.J., Lauer, G.P., Kothandaraman, R., O'Sullivan, E.J. and Trouilloud, P.L., 2016. Dependence of voltage and size on write error rates in spin-transfer torque magnetic random-access memory. *IEEE Magnetics Letters*, *7*, pp.1-4.

[25] Datta, S., Diep, V.Q. and Behin-Aein, B., 2014. What constitutes a nanoswitch? A Perspective. Emerging Nanoelectronic Devices. Hoboken, NJ, USA: Wiley, 2015, pp. 15–34.

[26] Vinasco, A. and Guillermo, J., 2014. Voltage-controlled magnetic dynamics in nanoscale magnetic tunnel junctions. Ph.D. dissertation, Dept. Elect. Eng., Univ. California, Los Angeles, CA, USA. [Online]. Available: https://escholarship.org/uc/item/6wm7x0rf.

[27] Niranjan, M.K., Duan, C.G., Jaswal, S.S. and Tsymbal, E.Y., 2010. Electric field effect on magnetization at the Fe/MgO (001) interface. *Applied Physics Letters*, *96*(22), p.222504.

[28] Bhattacharya, D. and Atulasimha, J., 2018. Skyrmion-mediated voltage-controlled switching of ferromagnets for reliable and energy-efficient two-terminal memory. *ACS applied materials & interfaces*, *10*(20), pp.17455-17462.

[29] Nakatani, Y., Hayashi, M., Kanai, S., Fukami, S. and Ohno, H., 2016. Electric field control of Skyrmions in magnetic nanodisks. *Applied Physics Letters*, *108*(15), p.152403.

[30] Bhattacharya, D., Al-Rashid, M.M. and Atulasimha, J., 2016. Voltage controlled core reversal of fixed magnetic skyrmions without a magnetic field. *Scientific reports*, *6*(1), pp.1-6.

[31] Bhattacharya, D., Razavi, S.A., Wu, H., Dai, B., Wang, K.L. and Atulasimha, J., 2020. Creation and annihilation of non-volatile fixed magnetic skyrmions using voltage control of magnetic anisotropy. *Nature Electronics*, *3*(9), pp.539-545.

[32] Je, S.G., Han, H.S., Kim, S.K., Montoya, S.A., Chao, W., Hong, I.S., Fullerton, E.E., Lee, K.S., Lee, K.J., Im, M.Y. and Hong, J.I., 2020. Direct demonstration of

topological stability of magnetic skyrmions via topology manipulation. *ACS nano*, *14*(3), pp.3251-3258.

[33] Yu, X.Z., Onose, Y., Kanazawa, N., Park, J.H., Han, J.H., Matsui, Y., Nagaosa, N. and Tokura, Y., 2010. Real-space observation of a two-dimensional skyrmion crystal. Nature, 465(7300), pp.901-904.

[34] Onose, Y., Okamura, Y., Seki, S., Ishiwata, S. and Tokura, Y., 2012. Observation of magnetic excitations of skyrmion crystal in a helimagnetic insulator Cu 2 OSeO 3. Physical review letters, 109(3), p.037603.

[35] Park, H.S., Yu, X., Aizawa, S., Tanigaki, T., Akashi, T., Takahashi, Y., Matsuda, T., Kanazawa, N., Onose, Y., Shindo, D. and Tonomura, A., 2014. Observation of the magnetic flux and three-dimensional structure of skyrmion lattices by electron holography. Nature nanotechnology, 9(5), pp.337-342.

[36] Heinze, S., Von Bergmann, K., Menzel, M., Brede, J., Kubetzka, A., Wiesendanger, R., Bihlmayer, G. and Blügel, S., 2011. Spontaneous atomic-scale magnetic skyrmion lattice in two dimensions. nature physics, 7(9), pp.713-718.

[37] Jiang, W., Upadhyaya, P., Zhang, W., Yu, G., Jungfleisch, M.B., Fradin, F.Y., Pearson, J.E., Tserkovnyak, Y., Wang, K.L., Heinonen, O. and Te Velthuis, S.G., 2015. Blowing magnetic skyrmion bubbles. Science, 349(6245), pp.283-286.

[38] Krause, S. and Wiesendanger, R., 2016. Skyrmionics gets hot. Nature materials, 15(5), pp.493-494.

[39] Li, J., Tan, A., Moon, K.W., Doran, A., Marcus, M.A., Young, A.T., Arenholz, E., Ma, S., Yang, R.F., Hwang, C. and Qiu, Z.Q., 2014. Tailoring the topology of an artificial magnetic skyrmion. Nature communications, 5(1), pp.1-6.

[40] Bogdanov, A.N. and Rößler, U.K., 2001. Chiral symmetry breaking in magnetic thin films and multilayers. *Physical review letters*, *87*(3), p.037203.

[41] Romming, N., Hanneken, C., Menzel, M., Bickel, J.E., Wolter, B., von Bergmann, K., Kubetzka, A. and Wiesendanger, R., 2013. Writing and deleting single magnetic skyrmions. *Science*, *341*(6146), pp.636-639.

[42] Mühlbauer, S., Binz, B., Jonietz, F., Pfleiderer, C., Rosch, A., Neubauer, A., Georgii, R. and Böni, P., 2009. Skyrmion lattice in a chiral magnet. *Science*, *323*(5916), pp.915-919.

[43] Hsu, P.J., Kubetzka, A., Finco, A., Romming, N., Von Bergmann, K. and Wiesendanger, R., 2017. Electric-field-driven switching of individual magnetic skyrmions. *Nature nanotechnology*, *12*(2), pp.123-126.

[44] Fert, A., Cros, V. and Sampaio, J., 2013. Skyrmions on the track. *Nature nanotechnology*, *8*(3), pp.152-156.

[45] Woo, S., Litzius, K., Krüger, B., Im, M.Y., Caretta, L., Richter, K., Mann, M., Krone, A., Reeve, R.M., Weigand, M. and Agrawal, P., 2016. Observation of room-temperature magnetic skyrmions and their current-driven dynamics in ultrathin metallic ferromagnets. Nature materials, 15(5), pp.501-506.

[46] Moreau-Luchaire, C., Moutafis, C., Reyren, N., Sampaio, J., Vaz, C.A.F., Van Horne, N., Bouzehouane, K., Garcia, K., Deranlot, C., Warnicke, P. and Wohlhüter, P., 2016. Additive interfacial chiral interaction in multilayers for stabilization of small individual skyrmions at room temperature. Nature nanotechnology, 11(5), pp.444-448.

[47] Boulle, O., Vogel, J., Yang, H., Pizzini, S., de Souza Chaves, D., Locatelli, A., Menteş, T.O., Sala, A., Buda-Prejbeanu, L.D., Klein, O. and Belmeguenai, M., 2016. Room-temperature chiral magnetic skyrmions in ultrathin magnetic nanostructures. Nature nanotechnology, 11(5), pp.449-454.

[48] Stebliy, M.E., Kolesnikov, A.G., Davydenko, A.V., Ognev, A.V., Samardak, A.S. and Chebotkevich, L.A., 2015. Experimental evidence of skyrmion-like configurations in bilayer nanodisks with perpendicular magnetic anisotropy. Journal of Applied Physics, 117(17), p.17B529.

[49] Dzyaloshinskii, I. E., 1957. Thermodynamic theory of "Weak" ferromagnetism in antiferromagnetic substances. Sov. Phys. JETP. 5, 1259.

[50] Moriya, T. New mechanism of anisotropic superexchange interaction., 1960. Phys. Rev. Lett. 4, 228–230.

[51] Moriya, T., 1960. Anisotropic superexchange interaction and weak ferromagnetism. Phys. Rev. 120, 91.

[52] Heide, M., Bihlmayer, G. & Blügel, S., 2008. Dzyaloshinskii-Moriya interaction accounting for the orientation of magnetic domains in ultrathin films: Fe/W(110). Phys. Rev. B 78, 140403.

[53] Pollard, S.D., Garlow, J.A., Yu, J., Wang, Z., Zhu, Y. and Yang, H., 2017. Observation of stable Néel skyrmions in cobalt/palladium multilayers with Lorentz transmission electron microscopy. Nature communications, 8(1), pp.1-8.

[54] Kézsmárki, I., Bordács, S., Milde, P., Neuber, E., Eng, L.M., White, J.S., Rønnow, H.M., Dewhurst, C.D., Mochizuki, M., Yanai, K. and Nakamura, H., 2015. Néel-type skyrmion lattice with confined orientation in the polar magnetic semiconductor GaV4S8. Nature materials, 14(11), pp.1116-1122.

[55] Yu, X.Z., Kanazawa, N., Onose, Y., Kimoto, K., Zhang, W.Z., Ishiwata, S., Matsui, Y. and Tokura, Y., 2011. D . Nature materials, 10(2), pp.106-109.

[56] Kang, W., Huang, Y., Zhang, X., Zhou, Y. and Zhao, W., 2016. Skyrmion-electronics: An overview and outlook. Proceedings of the IEEE, 104(10), pp.2040-2061.

[57] Everschor, K., Garst, M., Duine, R.A. and Rosch, A., 2011. Current-induced rotational torques in the skyrmion lattice phase of chiral magnets. *Physical Review B*, *84*(6), p.064401.

[58] Iwasaki, J., Mochizuki, M. and Nagaosa, N., 2013. Current-induced skyrmion dynamics in constricted geometries. *Nature nanotechnology*, *8*(10), pp.742-747.

[59] Nagaosa, N. and Tokura, Y., 2013. Topological properties and dynamics of magnetic skyrmions. *Nature nanotechnology*, *8*(12), pp.899-911.

[60] Tomasello, R., Martinez, E., Zivieri, R., Torres, L., Carpentieri, M. and Finocchio, G., 2014. A strategy for the design of skyrmion racetrack memories. Scientific reports, 4(1), pp.1-7.

[61] Sampaio, J., Cros, V., Rohart, S., Thiaville, A. and Fert, A., 2013. Nucleation, stability and current-induced motion of isolated magnetic skyrmions in nanostructures. Nature nanotechnology, 8(11), pp.839-844.

[62] Tolley, R., Montoya, S.A. and Fullerton, E.E., 2018. Room-temperature observation and current control of skyrmions in Pt/Co/Os/Pt thin films. *Physical Review Materials*, *2*(4), p.044404.

[63] Soumyanarayanan, A., Raju, M., Gonzalez Oyarce, A.L., Tan, A.K., Im, M.Y., Petrović, A.P., Ho, P., Khoo, K.H., Tran, M., Gan, C.K. and Ernult, F., 2017. Tunable room-temperature magnetic skyrmions in Ir/Fe/Co/Pt multilayers. *Nature materials*, *16*(9), pp.898-904.

[64] Büttner, F., Lemesh, I. and Beach, G.S., 2018. Theory of isolated magnetic skyrmions: From fundamentals to room temperature applications. *Scientific reports*, *8*(1), pp.1-12.

[65] Caretta, L., Mann, M., Büttner, F., Ueda, K., Pfau, B., Günther, C.M., Hessing, P., Churikova, A., Klose, C., Schneider, M. and Engel, D., 2018. Fast current-driven domain walls and small skyrmions in a compensated ferrimagnet. *Nature nanotechnology*, *13*(12), pp.1154-1160.

[66] Ma, C.T., Xie, Y., Sheng, H., Ghosh, A.W. and Poon, S.J., 2019. Robust formation of ultrasmall room-temperature Neél skyrmions in amorphous ferrimagnets from atomistic simulations. *Scientific reports*, *9*(1), pp.1-10.

[67] Vansteenkiste, A., Leliaert, J., Dvornik, M., Helsen, M., Garcia-Sanchez, F. and Van Waeyenberge, B., 2014. The design and verification of MuMax3. *AIP advances*, *4*(10), p.107133.

[68] Sampaio, J., Khvalkovskiy, A.V., Kuteifan, M., Cubukcu, M., Apalkov, D., Lomakin, V., Cros, V. and Reyren, N., 2016. Disruptive effect of Dzyaloshinskii-Moriya interaction on the magnetic memory cell performance. *Applied Physics Letters*, *108*(11), p.112403.

[69] Zhao, X., Zhang, B., Vernier, N., Zhang, X., Sall, M., Xing, T., Diez, L.H., Hepburn, C., Wang, L., Durin, G. and Casiraghi, A., 2019. Enhancing domain wall velocity through interface intermixing in W-CoFeB-MgO films with perpendicular anisotropy. *Applied Physics Letters*, *115*(12), p.122404.

[70] Zhang, X., Cai, W., Zhang, X., Wang, Z., Li, Z., Zhang, Y., Cao, K., Lei, N., Kang, W., Zhang, Y. and Yu, H., 2018. Skyrmions in magnetic tunnel junctions. *ACS applied materials & interfaces*, *10*(19), pp.16887-16892.

[71] Penthorn, N.E., Hao, X., Wang, Z., Huai, Y. and Jiang, H.W., 2019. Experimental observation of single skyrmion signatures in a magnetic tunnel junction. *Physical Review Letters*, *122*(25), p.257201.

[72] Zhang, X., Vernier, N., Zhao, W., Yu, H., Vila, L., Zhang, Y. and Ravelosona, D., 2018. Direct observation of domain-wall surface tension by deflating or inflating a magnetic bubble. *Physical Review Applied*, *9*(2), p.024032.

[73] Kozioł-Rachwał, A., Nozaki, T., Freindl, K., Korecki, J., Yuasa, S. and Suzuki, Y., 2017. Enhancement of perpendicular magnetic anisotropy and its electric field-induced change through interface engineering in Cr/Fe/MgO. *Scientific reports*, *7*(1), pp.1-11.

[74] Nozaki, T., Kozioł-Rachwał, A., Tsujikawa, M., Shiota, Y., Xu, X., Ohkubo, T., Tsukahara, T., Miwa, S., Suzuki, M., Tamaru, S. and Kubota, H., 2017. Highly efficient voltage control of spin and enhanced interfacial perpendicular magnetic anisotropy in iridium-doped Fe/MgO magnetic tunnel junctions. *NPG Asia Materials*, *9*(12), pp.e451-e451.

[75] Samardak, A., Kolesnikov, A., Stebliy, M., Chebotkevich, L., Sadovnikov, A., Nikitov, S., Talapatra, A., Mohanty, J. and Ognev, A., 2018. Enhanced interfacial Dzyaloshinskii-Moriya interaction and isolated skyrmions in the inversion-symmetry-broken Ru/Co/W/Ru films. *Applied Physics Letters*, *112*(19), p.192406.

[76] Cao, A., Zhang, X., Koopmans, B., Peng, S., Zhang, Y., Wang, Z., Yan, S., Yang, H. and Zhao, W., 2018. Tuning the Dzyaloshinskii–Moriya interaction in Pt/Co/MgO heterostructures through the MgO thickness. *Nanoscale*, *10*(25), pp.12062-12067.

[77] Cao, A., Chen, R., Wang, X., Zhang, X., Lu, S., Yan, S., Koopmans, B. and Zhao, W., 2020. Enhanced interfacial Dzyaloshinskii—Moriya interactions in annealed Pt/Co/MgO structures. *Nanotechnology*, *31*(15), p.155705.

[78] Kwon, S., Sun, Q., Mahfouzi, F., Wang, K.L., Amiri, P.K. and Kioussis, N., 2019. Voltage-controlled magnetic anisotropy in heterostructures with atomically thin heavy metals. *Physical Review Applied*, *12*(4), p.044075.

[79] Deger, C., 2020. Strain-enhanced dzyaloshinskii–moriya interaction at Co/Pt interfaces. *Scientific Reports*, *10*(1), pp.1-7.

[80] Yang, H., Boulle, O., Cros, V., Fert, A. and Chshiev, M., 2018. Controlling Dzyaloshinskii-Moriya interaction via chirality dependent atomic-layer stacking, insulator capping and electric field. *Scientific reports*, *8*(1), pp.1-7.

[81] Jan, G., Thomas, L., Le, S., Lee, Y.J., Liu, H., Zhu, J., Iwata-Harms, J., Patel, S., Tong, R.Y., Sundar, V. and Serrano-Guisan, S., 2018, June. Demonstration of ultra-low voltage and ultra low power STT-MRAM designed for compatibility with 0x node embedded LLC applications. In *2018 IEEE Symposium on VLSI Technology* (pp. 65-66). IEEE.

[82] Park, C., Lee, H., Ching, C., Ahn, J., Wang, R., Pakala, M. and Kang, S.H., 2018, June. Low RA magnetic tunnel junction arrays in conjunction with low switching current and high breakdown voltage for STT-MRAM at 10 nm and beyond. In *2018 IEEE Symposium on VLSI Technology* (pp. 185-186). IEEE.

[83] Cheng, H., Chen, J., Peng, S., Zhang, B., Wang, Z., Zhu, D., Shi, K., Eimer, S., Wang, X., Guo, Z. and Xu, Y., 2020. Giant Perpendicular Magnetic Anisotropy in Mo-Based Double-Interface Free Layer Structure for Advanced Magnetic Tunnel Junctions. *Advanced Electronic Materials*, *6*(8), p.2000271.

[84] Kato, Y., Yoda, H., Saito, Y., Oikawa, S., Fujii, K., Yoshiki, M., Koi, K., Sugiyama, H., Ishikawa, M., Inokuchi, T. and Shimomura, N., 2018. Giant voltage-controlled magnetic anisotropy effect in a crystallographically strained CoFe system. *Applied Physics Express*, *11*(5), p.053007.

[85] Munira, K., Xie, Y., Nadri, S., Forgues, M.B., Fashami, M.S., Atulasimha, J., Bandyopadhyay, S. and Ghosh, A.W., 2015. Reducing error rates in straintronic multiferroic nanomagnetic logic by pulse shaping. *Nanotechnology*, *26*(24), p.245202.

[86] Tanaka, G., Yamane, T., Héroux, J.B., Nakane, R., Kanazawa, N., Takeda, S., Numata, H., Nakano, D. and Hirose, A., 2019. Recent advances in physical reservoir computing: A review. *Neural Networks*, *115*, pp.100-123.

[87] Paquot, Y., Duport, F., Smerieri, A., Dambre, J., Schrauwen, B., Haelterman, M. and Massar, S., 2012. Optoelectronic reservoir computing. *Scientific reports*, *2*(1), pp.1-6.

[88] Vandoorne, K., Mechet, P., Van Vaerenbergh, T., Fiers, M., Morthier, G., Verstraeten, D., Schrauwen, B., Dambre, J. and Bienstman, P., 2014. Experimental demonstration of reservoir computing on a silicon photonics chip. *Nature communications*, *5*(1), pp.1-6.

[89] Marinella, M.J. and Agarwal, S., 2019. Efficient reservoir computing with memristors. *Nature Electronics*, *2*(10), pp.437-438.

[90] Torrejon, J., Riou, M., Araujo, F.A., Tsunegi, S., Khalsa, G., Querlioz, D., Bortolotti, P., Cros, V., Yakushiji, K., Fukushima, A. and Kubota, H., 2017. Neuromorphic computing with nanoscale spintronic oscillators. *Nature*, *547*(7664), pp.428-431.

[91] Rajib, M.M., Al Misba, W., Chowdhury, M.F.F., Alam, M.S. and Atulasimha, J., 2022. Skyrmion based energy-efficient straintronic physical reservoir computing. *Neuromorphic Computing and Engineering*, *2*(4), p.044011.